

**SIMULATIONS OF PROSTATE
BIOPSY METHODS**

by

Catherine Colby Pellish

B.S.E.E., Marquette University, 1985

A thesis submitted to the
University of Colorado at Denver
in partial fulfillment
of the requirements for the degree of
Master of Science
Applied Mathematics

1997

This thesis for the Master of Science

degree by

Catherine Pellish

has been approved

by

William L. Briggs

James R. Koehler

Weldon A. Lodwick

Date

Pellish, Catherine Colby (M.S., Applied Mathematics)

Simulations of Prostate Biopsy Methods

Thesis directed by Associate Professor William L. Briggs

Abstract

An accepted practice in screening for prostate cancer involves a needle core biopsy of the prostate gland, which can provide information regarding if, and how much, cancer is present in a gland. This paper documents several investigations into prostate gland biopsy techniques. The first phase of study involves a geometric model of a prostate gland containing one to three tumors. This mathematical model of the gland is then used to simulate various biopsy techniques and compare the resulting data. Secondly, the best biopsy procedure, as determined from the geometric model, is simulated on actual specimen data which have been digitized. These specimen data are also used for simulation of the six random systematic core biopsy technique (SRSCB) currently in clinical use. The results of the geometric model are compared to the results of the simulation on actual data. Finally, the geometric model is used in another series of simulations that investigate the number of needle samples needed to estimate the tumor to gland volume ratio.

This abstract accurately represents the content of the candidate's thesis. I recommend its publication.

Signed _____

William L. Briggs

ACKNOWLEDGEMENTS

I would like to sincerely thank a number of people who consistently provided me with their support, encouragement and guidance as I pursued the completion of this thesis. Dr. Bill Briggs, my advisor, served as a constant source of insight and motivation, as well as providing considerable direction throughout this process. I am also grateful for the time spent with Dr. Jim Koehler who had to teach me the finer points of statistics again and again. My thanks to both of these professors for proving to be excellent academic sources. I also would like to thank Norm LeMay who, out of the generosity of his heart and his need for a free lunch, assisted me in running the ANOVA analysis which this thesis required.

Finally, I must thank my family, Mark, Eric and Corinne for encouraging me and making me laugh through every crisis.

CONTENTS

Chapter

1	Introduction	2
1.1	Clinical Prostate Biopsy Analysis	2
1.2	Summary of Mathematical Methods	4
2	The Geometric Model	5
2.1	Geometric Model of gland and tumor	5
2.2	Simulations	10
2.3	Statistical Analysis of Results	14
2.4	Simulation Results	16
2.4.1	Applying the ANOVA to the Biopsy Simulation Data	18
2.4.2	ANOVA Mechanics	23
2.4.3	Residuals	24
2.4.4	The Null and Alternate Hypotheses	25
2.4.5	Are the Main Effects all Equal?	27
2.4.6	Recognizing Interaction between Factors	30
2.4.7	Clinical Distribution of Tumors	38

3	Digitized Specimen Data	43
3.1	Summary of Software Tool	43
3.2	Specific Algorithms	45
3.2.1	Locating the Apex	45
3.2.2	Establishing Needle Positions	47
3.3	Simulations	49
3.4	Geometric Model vs Clinical Model	51
3.5	Optimal Technique vs SRSCB	53
4	Geometric Model - Volume Estimates	56
4.1	Tumor Volume Estimates	56
4.1.1	One-Dimensional Analysis - Line Model	58
4.1.2	Two-Dimensional - Strip Model	58
4.1.3	Three-Dimensional - Cylinder Model	59
4.2	Experiment Setup	60
4.3	Results	62
4.4	Interactive Utility	63
 <u>Appendix</u>		
A	ANOVA Definitions	65

1. Introduction

1.1 Clinical Prostate Biopsy Analysis

Currently the standard method of determining if a given prostate gland is cancerous involves two procedures. The first is the prostate-specific antigen (PSA) test which measures the level of antigens in the patient's blood, a high level indicating a higher possibility of cancerous tissue. The second procedure is the needle biopsy which is carried out if the PSA test so indicates. The clinician conducts this biopsy by inserting a needle-tool, equipped with ultrasound capabilities, into the patient's rectum. The gland is located and the urologist fires three needles into the right lobe of the gland and three needles into the left lobe at approximately symmetric positions. The left-right division of the gland is determined by the position of the urethra in the gland. This physical landmark is used as the visual dividing line, enabling clinicians to execute the biopsy in a systematic manner. The needle-tool is rotated to the left or right depending on the targeted lobe. This rotation corresponds to the angle ϕ used in the mathematical analysis. Following this slight rotation, the needles are inserted at a second independent angle, referred

to as θ . The choice of a six-needle biopsy is based on the six random systematic core biopsies (SRSCB) method developed by Hodge et al [1] and currently thought to achieve the best detection rates.

The results from this diagnostic biopsy are then analyzed in order to determine the best treatment plan for the patient. There are several factors that help the urologist choose the optimal treatment plan. The first factor is obviously whether the biopsy shows any tumor cells at all. According to the Hodge study, 96% of the 83 men diagnosed with cancer had the cancer detected by SRSCB. However, as investigated by Daneshgari et al [2], in prostate glands with low tumor volume, the SRSCB fails to achieve such a high percentage of detection. This study concluded that “an improved biopsy strategy may be needed in detection of CaP (carcinoma of the prostate) in patients with low volume cancer”. Secondly, the volume of the tumor itself is a deciding factor in determining treatment. Thirdly, the location of the tumor, specifically if the tumor penetrates the capsule of the gland, can define a specific treatment plan. Some of this information is available from a single needle-core biopsy; more information is gleaned from successive, strategically placed biopsies.

1.2 Summary of Mathematical Methods

As an aid in understanding this problem, as well as researching ways to improve diagnosis, two methods of analysis are undertaken. The first method relies on a geometric model of the prostate gland with from one to three tumors. Various biopsy methods are simulated with this mathematical model and results are tabulated. The second method involves running the same biopsy simulations on actual prostate glands which have been digitized and stored as three-dimensional objects in a computer. The experimental results from these two methods are then compared. All of the simulations were executed using software created for this purpose primarily by this author, although the skeletons of these software tools were engineered during the Spring 1995 Math Clinic on this topic by several participants. The simulations are written in C and C++, running on a UNIX-based computer. They are extensively documented and flexible enough to be useful in a variety of experiments within this realm of research.

2. The Geometric Model

2.1 Geometric Model of gland and tumor

An actual prostate gland is about the size of a walnut with volumes ranging from 22 cc to 61 cc [3]. The geometry of an ellipsoid closely models this gland and any tumors present within it. Therefore, an ellipsoid of the form

$$\frac{x^2}{A^2} + \frac{y^2}{B^2} + \frac{z^2}{C^2} = 1,$$

is used to represent the prostate gland. Ellipsoids are also used to represent each of the tumors. The dimensions of the gland, A , B , and C , are chosen randomly in the following experimentally determined ranges:

- 3.0 cm < A < 4.8 cm
- 3.8 cm < B < 4.6 cm
- 3.8 cm < C < 5.2 cm
- 22 cc < [*gland volume*] < 61 cc.

The prostate is divided into 3 zones: the peripheral, the central and the transition region. The peripheral zone comprises approximately 70% of the mass of the prostate gland. It is located in the lower area of the gland,

closest to the rectum. This region is the “site of origin of most carcinomas” [3]. The central region makes up approximately 25% of the glandular mass and is “resistant to both carcinoma and inflammation” [3]. The transition region contains the remaining 5% of prostate gland tissue and can be the site of some cancers. Figure 2.1 shows these regions of the prostate gland. Based on this clinical information, the software-generated tumors are located in the lower part of the elliptical gland model to simulate tumors residing in the peripheral zone. Figure 2.2 depicts the geometrical gland and tumor model in the xyz system. Since the gland model is centered at the origin, the y -coordinate of the tumor center, y_c , is always negative in order to place the tumor in the peripheral zone of the gland. However, other distributions of y could be used to improve the model.

Tumors are modeled by an equation of the form

$$\frac{(x - x_c)^2}{a^2} + \frac{(y - y_c)^2}{b^2} + \frac{(z - z_c)^2}{c^2} = 1$$

where x_c , y_c and z_c specify the center of the tumor.

The biopsy needle is modeled as a line with the parametric equations

$$\begin{aligned} x(t) &= x_0 + t \sin \theta \sin \phi \\ y(t) &= y_0 + t \sin \theta \cos \phi \\ z(t) &= z_0 + t \cos \theta, \end{aligned}$$

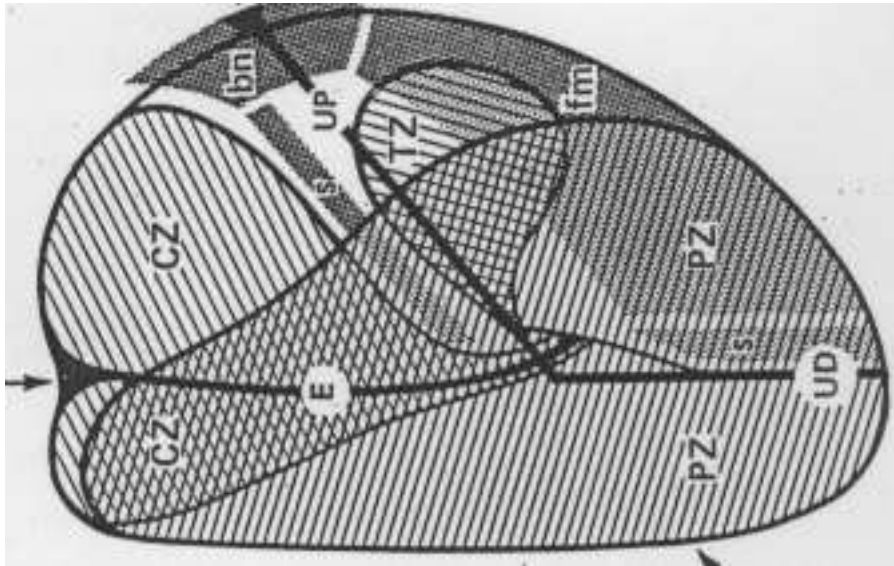


Figure 2.1. The peripheral (PZ), central (CZ) and transition (TZ) regions divide the prostate gland into 3 major zones.

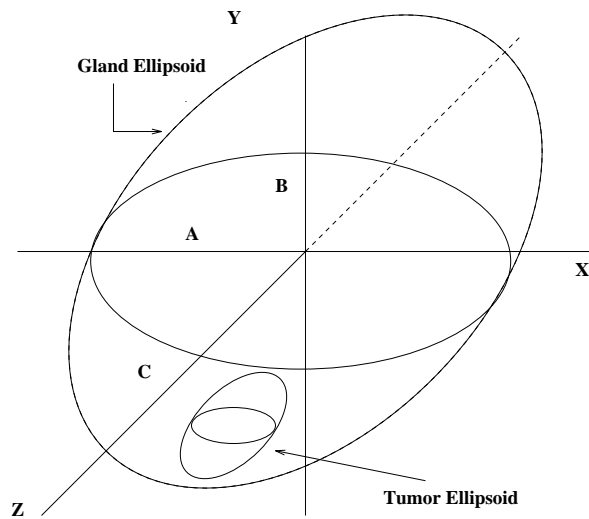


Figure 2.2. The gland and tumor are modeled by ellipsoids in the xyz coordinate system.

where x_0 , y_0 , and z_0 are the coordinates of the entry point of the needles (Figure 2.3 and Figure 2.4). The angle ϕ is measured from the y -axis and determines a plane. The angle θ is then assumed to remain in this plane and is measured from the z -axis. From these definitions, the parametric equations for the line are determined. The parameter t measures the length of the needle.

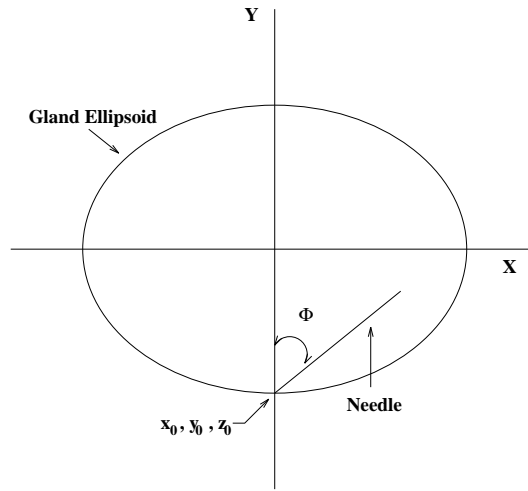


Figure 2.3. This figure of the xy plane and needle illustrates measurement of ϕ .

Substituting the parametric equations of the needle into the equation for the tumor, it is possible to determine values of t corresponding to an intersection.

The equation of the tumor is

$$\frac{(x(t) - x_c)^2}{a^2} + \frac{(y(t) - y_c)^2}{b^2} + \frac{(z(t) - z_c)^2}{c^2} = 1.$$

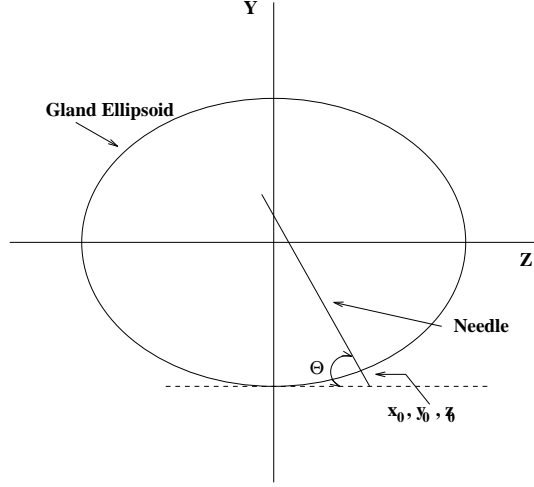


Figure 2.4. This figure of the yz plane and needle illustrates measurement of θ .

Replacing $x(t)$, $y(t)$ and $z(t)$ by the parametric equations of the needle gives

$$\begin{aligned}
 & t^2 \left(\frac{\sin^2 \phi \sin^2 \theta}{a^2} + \frac{\sin^2 \theta \cos^2 \phi}{b^2} + \frac{\cos^2 \theta}{c^2} \right) + \\
 & t \left(\frac{2(x_0 - x_c) \sin \phi \sin \theta}{a^2} + \frac{2(y_0 - y_c) \sin \theta \cos \phi}{b^2} + \right. \\
 & \left. \frac{2(z_0 - z_c) \cos \theta}{c^2} + \left(\frac{(x_0 - x_c)^2}{a^2} + \frac{(y_0 - y_c)^2}{b^2} + \frac{(z_0 - z_c)^2}{c^2} \right) \right) = 1. \quad (2.1)
 \end{aligned}$$

If the discriminant $(B'^2 - 4A'C')$ is positive, two real roots exist. In this case we have

$$\begin{aligned}
 A' &= \frac{\sin^2 \phi \sin^2 \theta}{a^2} + \frac{\sin^2 \theta \cos^2 \phi}{b^2} + \frac{\cos^2 \theta}{c^2} \\
 B' &= \frac{2(x_0 - x_c) \sin \phi \sin \theta}{a^2} + \frac{2(y_0 - y_c) \sin \theta \cos \phi}{b^2} + \frac{2(z_0 - z_c) \cos \theta}{c^2} \\
 C' &= \frac{(x_0 - x_c)^2}{a^2} + \frac{(y_0 - y_c)^2}{b^2} + \frac{(z_0 - z_c)^2}{c^2}.
 \end{aligned}$$

If real roots t_1 and t_2 exist, they give the points where the tumor ellipsoid and the line intersect. If these values are greater than 0 and less than the actual needle length, the needle has intersected the tumor. The amount of tumor extracted by the needle is proportional to the difference between the two roots of the quadratic, $|t_1 - t_2|$. By comparing the two roots, an estimate of the volume of the tumor that is contained in the needle can be made. If real roots do not exist, the needle does not intersect the tumor ellipsoid and no tumor information is gained by that needle.

In this analysis, each biopsy procedure was simulated on 1000 different gland models and the number of times a tumor was detected per procedure was recorded. This method does not differentiate between one or more needles detecting the tumor. It simply records a hit or miss per biopsy procedure. In addition, an estimate of the tumor volume is made whenever a tumor is detected.

2.2 Simulations

Since a fundamental goal of any biopsy is to determine whether or not the gland contains cancerous cells, the first series of simulations is intended to compare the detection rate of several biopsy techniques. The detection rate is defined as the number of times a biopsy procedure detects a tumor to the

total number of biopsies conducted. A set of 54 different biopsy procedures is simulated with variation in the following parameters: number of needles, offset between needles in the z direction, θ , and ϕ .

The distance in the z direction between needles can be a relative spacing based on the gland dimension in the z direction or an absolute spacing of 1 cm between each needle. The first method is referred to as **relative spacing** since it depends on the gland size and separates the needles by equal distance. The second is referred to as the **absolute spacing** and has its basis in the SRSCB procedure.

As a means of clarification, Figures 2.5 and 2.6 illustrate the analysis of a single specimen and the execution of the entire experiment. Each of the 54 biopsy procedures is simulated on 1000 different gland models. The random number generator is seeded once for each series of 1000 simulations using a specific biopsy technique. Prior to the next technique, the random number generator is reseeded with the same number, thereby yielding the identical set of 1000 prostate models. This insures that each of the biopsies is conducted on the same set of 1000 simulated glands. The detection rate is determined for each of these procedures and the results of the simulation are documented in Table 2.1.

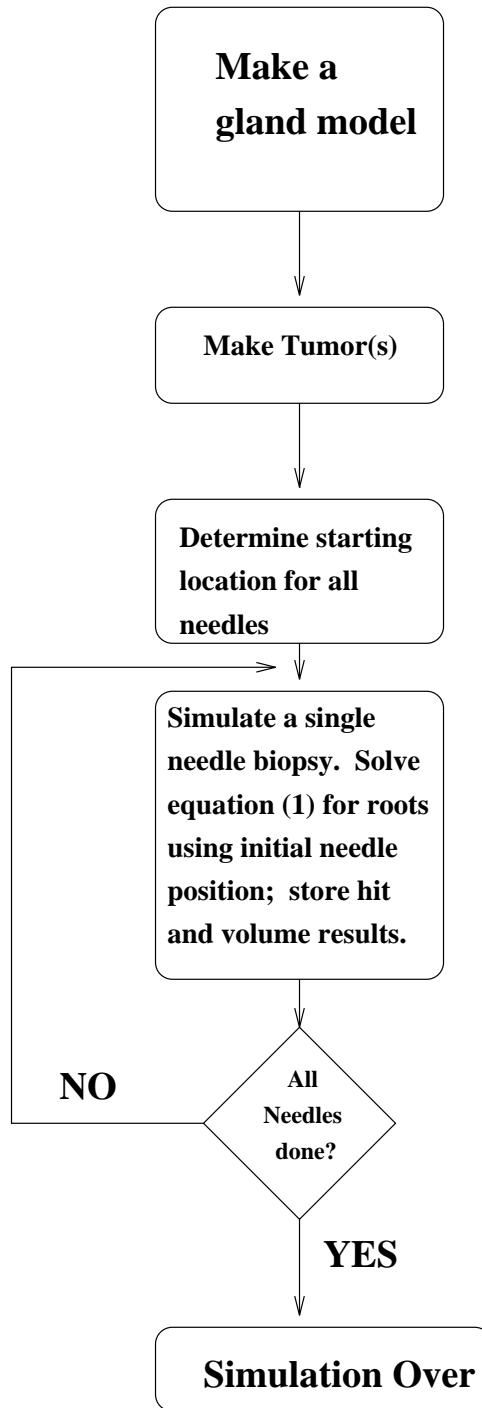


Figure 2.5. This flow chart depicts the top-level algorithm for modeling a single biopsy with several needles.

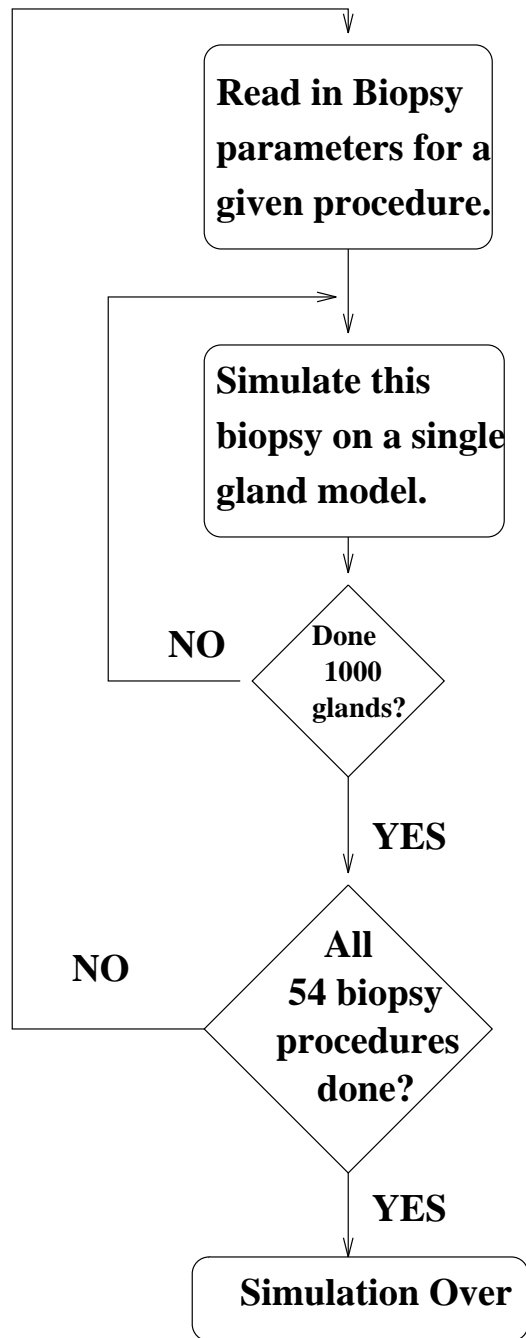


Figure 2.6. This flow chart depicts the simulation process for the entire simulation, each biopsy procedure is simulated on 1000 geometric gland models.

2.3 Statistical Analysis of Results

In order to interpret the output from the simulations legitimately, a statistical tool is needed. First, we must determine whether or not the various biopsy settings influence the observed detection rate. In other words, is there a relationship between the settings of any one or combination of the four factors (number of needles, z -spacing, θ and ϕ) and the detection rate or are the results completely random, therefore implying that the biopsy specification does not determine the detection rate? We need a mathematically sound method to compare the detection rates provided by the simulation and to infer some conclusions. The statistical model known as Analysis of Variance (ANOVA) was used to compare the population means between various treatments, thus resulting in a statistically valid conclusion. This model can be employed to determine whether the various factors interact and which factors have the most impact on the outcome.

In order to describe the ANOVA model, a few definitions are required.

(1) **Factors** are the independent variables that are under investigation.

In this instance, the biopsy parameters (number of needles, spacing

method, θ and ϕ) are the factors for the ANOVA model.

	Number of Needles	Spacing Method	θ	ϕ
Factor	4	Absolute	30°	30°
Levels	6	Relative	45°	45°
	8		60°	60°

- (2) **Factor levels** are the values that each of the factors can take on during a single simulation. As shown in the list of biopsy simulation factors and levels, each factor does not have the same number of factor levels. The factor **Spacing Method** only has two factor levels, whereas the other three factors each have three factor levels.
- (3) A **treatment** is a particular combination of levels of each of the factors involved in the **experiment**, where an **experiment** is the simulation of the treatment on 1000 geometric specimens. In this example, a treatment refers to a biopsy with specific settings (for example, 4 needles, absolute spacing, $\theta = 45^\circ$, $\phi = 45^\circ$). For the simulation, there are 54 different treatments and therefore, 54 different **experiments**, corresponding to all the combinations of the levels of the four factors.
- (4) A **trial** is defined to be a simulation of one treatment on one geometric model. The **outcome of a trial** is either 1, the biopsy procedure detected the tumor, or 0, the tumor remained undetected. The **outcome of the experiment** is the detection rate achieved by a specific

treatment simulated on 1000 geometric specimens. In other words, the **outcome of the experiment** is the number of specimens in which tumor is detected versus the total number of specimens simulated and is referred to as **outcome** for the remainder of this thesis.

2.4 Simulation Results

For each of the 54 treatments, the simulation is conducted on 1000 different gland models. The following table summarizes the treatment parameters as well as the results:

Experiment	Treatment Parameters			Outcome	
	Number of Needles	Spacing Method	θ	ϕ	Detection Rate
1	4	Relative	45°	45°	0.252
2	6	Relative	45°	45°	0.307
3	8	Relative	45°	45°	0.335
4	4	Absolute	45°	45°	0.263
5	6	Absolute	45°	45°	0.293
6	8	Absolute	45°	45°	0.298
7	4	Relative	60°	45°	0.267
8	6	Relative	60°	45°	0.341
9	8	Relative	60°	45°	0.369
10	4	Absolute	60°	45°	0.270
11	6	Absolute	60°	45°	0.320
12	8	Absolute	60°	45°	0.339
13	4	Relative	30°	45°	0.196
14	6	Relative	30°	45°	0.225
15	8	Relative	30°	45°	0.255
16	4	Absolute	30°	45°	0.207
17	6	Absolute	30°	45°	0.221
18	8	Absolute	30°	45°	0.221

Table 2.1. The results from the 54 geometric model experiments are displayed.

Experiment	Treatment Parameters			Outcome	
	Number of Needles	Spacing Method	θ	ϕ	Detection Rate
19	4	Relative	45°	60°	0.200
20	6	Relative	45°	60°	0.234
21	8	Relative	45°	60°	0.268
22	4	Absolute	45°	60°	0.211
23	6	Absolute	45°	60°	0.225
24	8	Absolute	45°	60°	0.228
25	4	Relative	60°	60°	0.191
26	6	Relative	60°	60°	0.254
27	8	Relative	60°	60°	0.268
28	4	Absolute	60°	60°	0.209
29	6	Absolute	60°	60°	0.240
30	8	Absolute	60°	60°	0.246
31	4	Relative	30°	60°	0.172
32	6	Relative	30°	60°	0.194
33	8	Relative	30°	60°	0.219
34	4	Absolute	30°	60°	0.188
35	6	Absolute	30°	60°	0.197
36	8	Absolute	30°	60°	0.197
37	4	Relative	45°	30°	0.260
38	6	Relative	45°	30°	0.316
39	8	Relative	45°	30°	0.341
40	4	Absolute	45°	30°	0.264
41	6	Absolute	45°	30°	0.305
42	8	Absolute	45°	30°	0.316
43	4	Relative	60°	30°	0.283
44	6	Relative	60°	30°	0.351
45	8	Relative	60°	30°	0.385
46	4	Absolute	60°	30°	0.279
47	6	Absolute	60°	30°	0.346
48	8	Absolute	60°	30°	0.372
49	4	Relative	30°	30°	0.210
50	6	Relative	30°	30°	0.247
51	8	Relative	30°	30°	0.273
52	4	Absolute	30°	30°	0.225
53	6	Absolute	30°	30°	0.245
54	8	Absolute	30°	30°	0.247

Table 2.1. (Cont.) The results from the 54 geometric model experiments are displayed.

2.4.1 Applying the ANOVA to the Biopsy Simulation Data

The biopsy simulation is a multi-factored system, in which the four parameters (number of needles, spacing, θ and ϕ) individually and perhaps in some combinations may have a measurable effect on the detection rate. Therefore a factor effects model is used in order to determine the impact of and interactions between these four parameters. This biopsy simulation is considered a complete factorial study since all possible combinations of the four parameters were simulated and evaluated. The indices i, j, k, l refer to the levels of the factors *number of needles*, *spacing method*, θ and ϕ , respectively.

In this multi-factored system, a true overall mean, μ which is equivalent to the true overall detection rate, is assumed to exist. The entire simulation results in 54 observed detection rates, p_{ijkl} , each of which indicates the observed detection rate for a given experiment. This set of 54 observed detection rates is used in the ANOVA to determine estimated factor effects and an estimated overall mean which are used in the factor effects model. The factor effects model is used to predict a detection rate, a probability of detection, \hat{p}_{ijkl} , given the levels of the four factors.

A **factor level mean** is the average detection rate for a group of

treatments that have one common factor level held constant while all others vary. For example, all outcomes from experiments with *Number of Needles*= 6 are averaged to yield the factor level mean for the factor *Number of Needles* at the level $i = 6$. The **overall mean**, μ , is simply the average outcome of all experiments. The difference between each factor level mean and the overall mean yields the **main effect** for that factor level. Because this model has 4 factors each with either 2 or 3 levels, the following **main effects** are designated.

- α_i - the main effect for the factor *Number of Needles* at each of its levels (4,6,8): $1 \leq i \leq 3$.
- β_j - the main effect for the factor *Spacing Method* at each of its levels (0,1): $1 \leq j \leq 2$.
- γ_k - the main effect for the factor θ at each of its levels (30°,45°,60°): $1 \leq k \leq 3$.
- δ_l - the Main Effect for the factor ϕ at each of its levels (30°,45°,60°): $1 \leq l \leq 3$.

A factor at a particular level may influence another factor either by inhibiting or enhancing its impact. Because of these interactions between factors, the interaction effects are included in the model. Pairwise interaction

effects are a measure of the combined effect of two factors, across the different levels, minus the main effects of these factors. We define these two-way effects as follows.

- $(\alpha\beta)_{ij}$ - number of needles and spacing method
- $(\alpha\gamma)_{ik}$ - number of needles and θ
- $(\alpha\delta)_{il}$ - number of needles and ϕ
- $(\beta\gamma)_{jk}$ - spacing method and θ
- $(\beta\delta)_{jl}$ - spacing method and ϕ
- $(\gamma\delta)_{kl}$ - θ and ϕ .

Three-way factor effects are a measure of the interaction effect of three factors.

- $(\alpha\beta\gamma)_{ijk}$ - number of needles, spacing method and θ
- $(\alpha\beta\delta)_{ijl}$ - number of needles, spacing method and ϕ
- $(\beta\gamma\delta)_{jkl}$ - spacing method, θ and ϕ
- $(\alpha\gamma\delta)_{ikl}$ - number of needles, θ and ϕ .

The four-way effect is the measure of the interaction effect of all four factors.

- $(\alpha\beta\gamma\delta)_{ijkl}$ - number of needles, spacing method, θ and ϕ .

Summary of Variables	
True overall mean	μ
Estimated overall mean	$\hat{\mu}$
True treatment mean	μ_{ijkl}
Estimated treatment mean	$\hat{\mu}_{ijkl}$
Observed treatment detection rate	p_{ijkl}
Transformed observed treatment detection rate	Y_{ijkl}
Estimated treatment detection rate	\hat{p}_{ijkl}
Transformed estimated treatment detection rate	\hat{Y}_{ijkl}
Average observed detection rate	\bar{p}
True main factor level effects	$\alpha_i, \beta_j, \gamma_k, \delta_l$
Estimated main factor level effects	$\hat{\alpha}_i, \hat{\beta}_j, \hat{\gamma}_k, \hat{\delta}_l$
True two-way effects	$(\alpha\beta)_{ij}, (\alpha\gamma)_{ik}, (\alpha\delta)_{il}$ $(\beta\gamma)_{jk}, (\beta\delta)_{jl}, (\gamma\delta)_{kl}$
Estimated two-way effects	$(\widehat{\alpha\beta})_{ij}, (\widehat{\alpha\gamma})_{ik}, (\widehat{\alpha\delta})_{il}$ $(\widehat{\beta\gamma})_{jk}, (\widehat{\beta\delta})_{jl}, (\widehat{\gamma\delta})_{kl}$

Table 2.2. A list of the variables used in the ANOVA analysis is displayed.

The factor effects model takes the general form

$$\begin{aligned} \mu_{ijkl} = & \mu + \alpha_i + \beta_j + \gamma_k + \delta_l + (\alpha\beta)_{ij} + (\alpha\gamma)_{ik} + (\alpha\delta)_{il} + (\beta\gamma)_{jk} + (\beta\delta)_{jl} + (\gamma\delta)_{kl} \\ & + (\alpha\beta\gamma)_{ijk} + (\alpha\beta\delta)_{ijl} + (\beta\gamma\delta)_{jkl} + (\alpha\gamma\delta)_{ikl} + (\alpha\beta\gamma\delta)_{ijkl}. \end{aligned}$$

The observed outcome, the detection rate for a particular treatment, as given in Table 2.1, is p_{ijkl} and is the sum of the true mean for that treatment and a residual term:

$$p_{ijkl} = \mu_{ijkl} + \varepsilon_{ijkl}.$$

The goal of the analysis is to formulate a model that predicts the outcome of a given treatment. Since the true means and true factor effects are not known, estimates of these terms are determined from the simulation and used in the model. Estimated values are indicated with the $\hat{\cdot}$ notation. The predicted outcome \hat{p}_{ijkl} is represented by the following relationship:

$$\begin{aligned} \hat{p}_{ijkl} = & \hat{\mu} + \hat{\alpha}_i + \hat{\beta}_j + \hat{\gamma}_k + \hat{\delta}_l + (\widehat{\alpha\beta})_{ij} + (\widehat{\alpha\gamma})_{ik} + (\widehat{\alpha\delta})_{il} + (\widehat{\beta\gamma})_{jk} + (\widehat{\beta\delta})_{jl} + (\widehat{\gamma\delta})_{kl} \\ & + (\widehat{\alpha\beta\gamma})_{ijk} + (\widehat{\alpha\beta\delta})_{ijl} + (\widehat{\beta\gamma\delta})_{jkl} + (\widehat{\alpha\gamma\delta})_{ikl} + (\widehat{\alpha\beta\gamma\delta})_{ijkl}. \end{aligned}$$

In this equation \hat{p}_{ijkl} is the estimated probability of detecting a tumor at the factor levels indicated by i, j, k, l . This probability is predicted by the model using least -square estimators for the terms in the equation. The probability of detection is a function of the estimated overall mean, $\hat{\mu}$, and the estimated effects from the four factors, alone and in combination with one another. Not all of these effects may be significant. In order to determine which of the factors do significantly effect the detection rate and therefore belong in the final model, various means are evaluated. If all the means for a particular factor (or combination of factors) are equal, varying a factor level does not add to or subtract from the overall mean and therefore the factor does not belong in the final model. This equality question is put, not only to each factor individually, but to all the combinations of factors as well.

2.4.2 ANOVA Mechanics

Use of the ANOVA model is founded on several assumptions:

- (1) The outcomes follow a normal probability distribution.
- (2) Each distribution has the same variance.
- (3) The outcomes for each factor level are independent of the other factor level outcomes.

With these assumptions in mind, note that the probability distributions of a factor at each of its levels differs only with respect to the mean [4]. Therefore, the first step in executing the analysis is to determine if the detection rates, are statistically different. Secondly, if they are different, one of the intents of the ANOVA model is to determine if the difference between the detection rate of two or more treatments is sufficient, after examining the variability within the treatments, to conclude that one treatment does indeed produce a higher detection rate. In addition, by evaluating the statistical data, conclusions may be drawn as to how each factor, both independently and within established interaction groups (pairwise, three-way or four-way), influences the outcome.

2.4.3 Residuals

We define \bar{p} to be the average of all observations. The model states that $p_{ijkl} = \mu_{ijkl} + \varepsilon_{ijkl}$; therefore the residual term is $\varepsilon_{ijkl} = p_{ijkl} - \mu_{ijkl}$. Since μ_{ijkl} is estimated by $\hat{\mu}_{ijkl}$, the estimated residual term is $e_{ijkl} = p_{ijkl} - \hat{\mu}_{ijkl}$, the difference between the observed and the estimated average detection rate. The set of all 54 residuals, e_{ijkl} , for all i, j, k and l are evaluated for three characteristics which indicate whether the fitted data are well-suited for the analysis. These characteristics are:

1. Normality of error terms.
2. Constancy of error variance.
3. Independence of error terms.

Several statistical tests and plots used on the residual data determine whether one of the five assumptions is violated. These tests revealed that the error variances were not stable, thus violating the first characteristic. A transformation was employed to preserve the statistical information in the output, but stabilize the error variances. Since nothing is lost by employing a transformation and the error variances are stabilized, the detection rate data p is transformed to Y via the following relationship:

$$Y = 2 \arcsin(\sqrt{p}).$$

The outcome from these simulations is the detection rate, a proportion of the number of specimens where tumor is detected to the total number of specimens. The arcsine transformation is the most appropriate transformation when the outcome is a proportion [4]. All ANOVA data referenced from this point on are transformed unless noted otherwise. The inverse transformation is calculated at the conclusion of this analysis to get a true estimate of the probability.

2.4.4 The Null and Alternate Hypotheses

A starting point in the ANOVA process is to establish two hypothesis, a null and alternate hypothesis. The null hypothesis assumes that all effects are equal, therefore indicating that specific factor levels do not influence the outcome. The alternate hypothesis assumes that at least two of the effects are not the same.

The F-test is used to decide which of these two hypotheses concerning the data will be accepted. The test consists of computing the ratio of between-effect variation to within-effect variation. This between-effect variation, which changes depending on the effect, is called the **treatment sum of squares** and is denoted SSA , SSB , SSC , and SSD (see Appendix also). It is a measure of the difference between the detection rate of a set of treatments and the average detection rate over all treatments. The within-effect variation

is called the **error sum of squares** and is denoted SSE . It is a measure of the difference between the individual outcome for a given treatment and the estimated detection rate over that treatment. The error sum of squares measures variability that is not explained by the SSA , SSB , SSC , or SSD terms and therefore occurs within the set of treatments. Both of these variation measurements are evaluated using sum of the squares expressions as detailed in the Appendix. The means of the SSA , SSB , SSC , SSD and SSE terms are MSA , MSB , MSC , MSD and MSE respectively, and are computed by dividing by the degrees of freedom, df , associated with each term. This results in $F = MSA/MSE$ where $MSA = SSA/df_A$ ($MSB = SSB/df_B$, etc) and $MSE = SSE/df$. Large values of F tend to support the conclusion that all the effects are not equal (H_a), whereas values of F near 1 support the null hypothesis (H_0). In the event that the alternate hypothesis is indicated via the F-test, the ANOVA also provides the probability of a **TYPE I** error. A **TYPE I** error occurs when it is concluded that differences between means exist when, in fact, they do not (i.e. accept H_a when in fact H_o is true). This information is given in the column labelled $Pr(F)$ in the ANOVA output in Table 2.3.

2.4.5 Are the Main Effects all Equal?

Following the general process of establishing null and alternate hypothesis as described above, a pair of null and alternate hypotheses are stated for each factor in the biopsy model. The null hypothesis assumes that the main effects for a given factor at each of its levels are equivalent. The alternate hypothesis obviously assumes that the main effects differ.

$$\begin{array}{ll} H_0: & \alpha_1 = \alpha_2 = \alpha_3 \quad H_a: \quad \text{not all } \alpha_i \text{ are equal.} \\ & \beta_1 = \beta_2 \quad \text{not all } \beta_i \text{ are equal.} \\ & \delta_1 = \delta_2 = \delta_3 \quad \text{not all } \gamma_i \text{ are equal.} \\ & \gamma_1 = \gamma_2 = \gamma_3 \quad \text{not all } \delta_i \text{ are equal.} \end{array}$$

The F-test statistic is applied to determine which hypothesis to accept in each case. The factor sum of squares for each factor, number of needles, spacing, θ and ϕ , denoted SSA , SSB , SSC and SSD , respectively, is computed as shown in the Appendix. The mean of each of these factor sum of square terms is computed by dividing each term by its associated degrees of freedom so that $MSA = SSA/df_A$, $MSB = SSB/df_B$, etc. as detailed in the Appendix. The test statistic is formed for each hypothesis in the following manner. To test the effect of the first factor, Number of Needles, $F = MSA/MSE$; to test the effect of the spacing factor,

$F = MSB/MSE$; to test the effect of θ , $F = MSC/MSE$; and to test the effect of ϕ , $F = MSD/MSE$. Accepting the alternate hypothesis means that a specific setting of the given factor corresponds to a change in detection rate; thus that factor has an effect on the overall outcome of the biopsy.

		Df	Sum of Sq	Mean Sq	F Value	Pr(F)
Main Effects	Needles	2	0.15862	0.07931	607.427	0.0000000
	Spacing	1	0.00498	0.00498	38.209	0.0000011
	θ	2	0.29249	0.14624	1120.073	0.0000000
	ϕ	2	0.28115	0.14057	1076.661	0.0000000
2-Way Effects	Ndls:Spc	2	0.1641	0.00820	62.846	0.0000000
	Needles: θ	4	0.01444	0.00361	27.653	0.0000000
	Spacing: θ	2	0.00059	0.00029	2.283	0.1206068
	Needles: ϕ	4	0.00395	0.00098	7.569	0.0002892
	Spacing: ϕ	2	0.00046	0.00023	1.794	0.1848710
	θ: ϕ	4	0.02867	0.00716	54.902	0.0000000
Residuals	28	0.00365	0.00013			

Table 2.3. The output from the ANOVA is displayed above. See Appendix for details of the calculations.

Referring to this ANOVA output, the column of numbers labelled Sum of Sq refers to the parameters SSA, SSB, SSC and SSD detailed in the Appendix. The column labelled Mean Square lists the parameters MSA, MSB, MSC, MSD. The F Value column lists the F-test outcome for each row: (**Needles** F Value = MSA/MSE). The larger values in this column tend to support the alternate hypothesis that the main effect for a given factor differs across

the possible levels for that factor. The final column, $\Pr(F)$, gives the probability of a Type I error. Again, a Type I error occurs if the alternate hypothesis is concluded when in fact, the null hypothesis is true. The row labelled Residuals indicates the total degrees of freedom, the SSE and the MSE for this analysis.

Based on the numbers in the table, each of the four main effects has a significant effect on the outcome with the factor θ having the greatest influence on the detection rate, followed by the factors ϕ and **Number of Needles**. This fact is indicated by the high F-value that corresponds to each of the four factors. The rows labelled with two factor names (for example, **Needles: Spacing**) indicate the ANOVA output corresponding to pair-wise interactions and include the sum of squares computed for each pair of factors. The sum of squares for all of the pair-wise interaction terms ($SSAB, SSAC, SSAD, SSBC, SSBD, SSCD$) are computed as detailed in the Appendix. The total treatment sum of squares, $SSTR = SSA + SSB + SSC + SSD + SSAB + SSAC + SSAD + SSBC + SSBD + SSCD$. This sum does not include the sum of square terms due to the three-way and four-way interactions because there are not enough degrees of freedom in the experiment to use the full model.

2.4.6 Recognizing Interaction between Factors

At this point, the F-test has determined that each of the main factor effects contributes to the overall detection rate. To evaluate the interaction effects, the F-test is applied again. The F-test is applied to determine interaction between, in this case, two, three or four factors. A null and alternate hypothesis is formulated for all possible combinations of factors and sum of square terms are computed for the factor groups and used in each F-test. The null and alternate hypothesis are constructed for each of the pairwise interactions.

$$\begin{array}{ll}
 H_0: & \text{all } (\alpha\beta)_{ij} = 0 \\
 & \text{all } (\alpha\gamma)_{ik} = 0 \\
 & \text{all } (\alpha\delta)_{il} = 0 \\
 & \text{all } (\beta\gamma)_{jk} = 0 \\
 & \text{all } (\beta\delta)_{jl} = 0 \\
 & \text{all } (\gamma\delta)_{kl} = 0 \\
 H_a: & \text{not all } (\alpha\beta)_{ij} = 0 \\
 & \text{not all } (\alpha\gamma)_{ik} = 0 \\
 & \text{not all } (\alpha\delta)_{il} = 0 \\
 & \text{not all } (\beta\gamma)_{jk} = 0 \\
 & \text{not all } (\beta\delta)_{jl} = 0 \\
 & \text{not all } (\gamma\delta)_{kl} = 0
 \end{array}$$

All three-way combinations are formed, hypotheses are constructed and F-test results are evaluated.

$$\begin{array}{ll}
 H_0: & \text{all } (\alpha\beta\gamma)_{ijk} = 0 \\
 & \text{all } (\alpha\beta\delta)_{ijl} = 0 \\
 & \text{all } (\alpha\gamma\delta)_{ikl} = 0 \\
 & \text{all } (\beta\gamma\delta)_{jkl} = 0 \\
 H_a: & \text{not all } (\alpha\beta\gamma)_{ijk} = 0 \\
 & \text{not all } (\alpha\beta\delta)_{ijl} = 0 \\
 & \text{not all } (\alpha\gamma\delta)_{ikl} = 0 \\
 & \text{not all } (\beta\gamma\delta)_{jkl} = 0
 \end{array}$$

The null/alternate set of hypothesis is constructed for the four-way interaction.

$$H_0: \text{ all } (\alpha\beta\gamma\delta)_{ijkl} = 0$$

$$H_a: \text{ not all } (\alpha\beta\gamma\delta)_{ijkl} \text{ equal } 0$$

Based on the actual ANOVA results in the preceding table, four of the pair-wise interactions appear strongly significant: **Needles: Spacing**, **Needles: θ** , **Needles: ϕ** and **θ : ϕ** . The other two pair-wise interactions are included in the final model even though the strength of their significance is uncertain. The ANOVA was executed once to include all three-way interactions. Since these interactions proved insignificant, they are not included in the model. There are not enough degrees of freedom in the experiment to estimate the residuals and test for the four-way interaction.

As stated previously, the Y notation indicates the transformed detection rate (p). At this point the general model, of the form

$Y_{ijklm} = \mu_{\dots} + \alpha_i + \beta_j + \gamma_k + \delta_l$	Main effects
$+ (\alpha\beta)_{ij} + (\alpha\gamma)_{ik} + (\alpha\delta)_{il} + (\beta\gamma)_{jk} + (\beta\delta)_{jl} + (\gamma\delta)_{kl}$	Pairwise effects
$+ (\alpha\beta\gamma)_{ijk} + (\alpha\beta\delta)_{ijl} + (\beta\gamma\delta)_{jkl}$	Three-way effects
$+ (\alpha\beta\gamma\delta)_{ijkl}$	Four-way effect
$+ \epsilon_{ijklm}$	residual error

is reduced to the final model for this analysis:

$$\hat{Y}_{ijkl} = \hat{\mu} + \hat{\alpha}_i + \hat{\beta}_j + \hat{\gamma}_k + \hat{\delta}_l + (\widehat{\alpha\beta})_{ij} + (\widehat{\alpha\gamma})_{ik} + (\widehat{\alpha\delta})_{il} + (\widehat{\beta\gamma})_{jk} + (\widehat{\beta\delta})_{jl} + (\widehat{\gamma\delta})_{kl}.$$

This model yields the transformed probability of detection at the given levels for i, j, k and l .

Now that the factor effects have been identified, the analysis revolves around determining the factor levels that result in the highest detection rate. For this part of the analysis, the tables of means and tables of effects are evaluated.

$\mu_{...}$	Grand Mean 1.072				
Needles	4	6	8	Spacing	Relative Absolute
$\mu_{i...}$	0.999	1.09	1.128	$\mu_{.j..}$	1.082 1.063
θ	30°	45°	60°	ϕ	30° 45° 60°
$\mu_{..k.}$	0.9723	1.098	1.147	$\mu_{...l}$	1.14 1.1104 0.9724

Table 2.4. The ANOVA tables of means list the transformed values.

Needles	θ			Spacing	θ		
	30°	45°	60°		30°	45°	60°
4	0.926	1.027	1.045	Relative	0.978	1.111	1.157
6	0.979	1.113	1.176	Absolute	0.967	1.084	1.137
8	1.012	1.152	1.221				
Needles	ϕ			Spacing	ϕ		
	30°	45°	60°		30°	45°	60°
4	1.054	1.028	0.915	Relative	1.148	1.118	0.980
6	1.161	1.123	0.985	Absolute	1.132	1.091	0.965
8	1.205	1.163	1.017				
Needles	Spacing		θ	ϕ			
	Relative	Absolute		30°	45°	60°	
4	0.987	1.011	30°	1.026	0.978	0.913	
6	1.099	1.080	45°	1.159	1.139	.0994	
8	1.159	1.097	60°	1.235	1.196	1.010	

Table 2.5. The transformed values of the pairwise means are shown.

Referring to the ANOVA tables of means, the highest numbers in each category reflect the best setting for a particular factor. On reading through the tables of means, the conclusion is that a technique of 8 needles, relative spacing, $\theta = 60^\circ$ and $\phi = 30^\circ$ yields the best detection rate. In order to corroborate this more fully, the interactions that are deemed significant are analysed to verify that the main effect is not contradicted by an interaction. Therefore, the table for **Needles: θ** is reviewed and it is found that the setting of 8 needles and $\theta = 60^\circ$ again yields the highest mean. The tables for all of the pair-wise combinations are reviewed to determine that the best settings yield the highest means in the interaction tables just as they did in the main effect tables. This proves to be the case, so none of the interactions contradict the conclusion drawn from the main effect information.

Number of Needles (4, 6, or 8)	$\hat{\alpha}_1$	$\hat{\alpha}_2$	$\hat{\alpha}_3$
Effect	-0.07329	0.01723	0.05607
Spacing (Relative or Absolute)	$\hat{\beta}_1$	$\hat{\beta}_2$	
Effect	0.009612	-0.009612	
θ (30°, 45°, or 60°)	$\hat{\gamma}_1$	$\hat{\gamma}_2$	$\hat{\gamma}_3$
Effect	-0.1001	0.02519	0.07486
ϕ (30°, 45°, or 60°)	$\hat{\delta}_1$	$\hat{\delta}_2$	$\hat{\delta}_3$
Effect	0.0678	0.03215	-0.09995

Table 2.6. The main factor level effects from the ANOVA output are documented.

		Spacing		
		Relative	Absolute	
Needles	4	-0.02127	0.02127	
	6	-0.00017	0.00017	
	8	0.02143	-0.02143	
		θ		
		30°	45°	60°
Needles	4	0.02680	0.00244	-0.02925
	6	-0.01031	-0.00127	0.01158
	8	-0.01649	-0.00118	0.01767
		θ		
		30°	45°	60°
Spacing	Relative	-0.004354	0.003708	0.000646
	Absolute	0.004354	-0.003708	-0.000646
		ϕ		
		30°	45°	60°
Needles	4	-0.01271	-0.00292	0.01563
	6	0.00363	0.00087	-0.00450
	8	0.00907	0.00206	-0.01113
		ϕ		
		30°	45°	60°
Spacing	Relative	-0.001740	0.004148	-0.002407
	Absolute	0.001740	-0.004148	0.002407
		ϕ		
		30°	45°	60°
θ	30°	-0.01404	-0.02664	0.04067
	45°	-0.00621	0.00978	-0.00357
	60°	0.02025	0.01686	-0.03711

Table 2.7. The ANOVA table of effects for pairwise interactions is displayed.

By using the values from the tables of effects, a probability for detection is calculated for the optimal setting:

$$\hat{Y}_{3131} = \hat{\mu} + \hat{\alpha}_3 + \hat{\beta}_1 + \hat{\gamma}_3 + \hat{\delta}_1 + (\widehat{\alpha\beta})_{31} + (\widehat{\alpha\gamma})_{33} + (\widehat{\alpha\delta})_{31} + (\widehat{\beta\gamma})_{13} + (\widehat{\beta\delta})_{11} + (\widehat{\gamma\delta})_{31}$$

$$1.347918 = 1.072 + .05607 + .009612 + .07486 + .0678 +$$

$$.02143 + .01767 + .00907 + .000646 + -0.00174 + .02025$$

This result of 1.347918 is then transformed back (arcsine equation) to yield a probability of 0.38948 for this setting.

$$1.347918 = 2 \arcsin \sqrt{(p)}$$

$$p = (\sin(1.347918/2))^2 = 0.38949.$$

Therefore, with the factors set to 8 needles, relative spacing, $\theta = 60^\circ$ and $\phi = 30^\circ$, the biopsy procedure has a 38.9% probability of detecting the cancer given the tumor distribution model used. This estimated probability is best used in comparisons with the other estimated probabilities rather than as an absolute measure of detection rate. Therefore the conclusion from this analysis is a relative ranking of treatments in terms of their detection rate. Since the 1000 simulated specimens were the same for each treatment, the ANOVA model determined the relative differences between detection rates of various treatments, not necessarily providing enough data and results to draw

conclusions about absolute detection rates. Table 2.8 lists each experiment and the probability of detection predicted from the factor effects model.

Experiment	Treatment		Parameters		Predicted Probability
	Number of Needles	Spacing Method	θ	ϕ	
1	4	Relative	45°	45°	0.247
2	6	Relative	45°	45°	0.297
3	8	Relative	45°	45°	0.327
4	4	Absolute	45°	45°	0.251
5	6	Absolute	45°	45°	0.281
6	8	Absolute	45°	45°	0.291
7	4	Relative	60°	45°	0.265
8	6	Relative	60°	45°	0.337
9	8	Relative	60°	45°	0.369
10	4	Absolute	60°	45°	0.271
11	6	Absolute	60°	45°	0.324
12	8	Absolute	60°	45°	0.335
13	4	Relative	30°	45°	0.195
14	6	Relative	30°	45°	0.227
15	8	Relative	30°	45°	0.251
16	4	Absolute	30°	45°	0.205
17	6	Absolute	30°	45°	0.219
18	8	Absolute	30°	45°	0.224
19	4	Relative	45°	60°	0.200
20	6	Relative	45°	60°	0.236
21	8	Relative	45°	60°	0.260
22	4	Absolute	45°	60°	0.208
23	6	Absolute	45°	60°	0.227
24	8	Absolute	45°	60°	0.232
25	4	Relative	60°	60°	0.192
26	6	Relative	60°	60°	0.247
27	8	Relative	60°	60°	0.273
28	4	Absolute	60°	60°	0.203
29	6	Absolute	60°	60°	0.241

Table 2.8. The probabilities of detection for one tumor simulations are displayed.

	Treatment		Parameters		
Experiment	Number of Needles	Spacing Method	θ	ϕ	Predicted Probability
30	8	Absolute	60°	60°	0.248
31	4	Relative	30°	60°	0.175
32	6	Relative	30°	60°	0.196
33	8	Relative	30°	60°	0.215
34	4	Absolute	30°	60°	0.189
35	6	Absolute	30°	60°	0.194
36	8	Absolute	30°	60°	0.195
37	4	Relative	45°	30°	0.257
38	6	Relative	45°	30°	0.314
39	8	Relative	45°	30°	0.346
40	4	Absolute	45°	30°	0.266
41	6	Absolute	45°	30°	0.303
42	8	Absolute	45°	30°	0.315
43	4	Relative	60°	30°	0.276
44	6	Relative	60°	30°	0.354
45	8	Relative	60°	30°	0.389
46	4	Absolute	60°	30°	0.287
47	6	Absolute	60°	30°	0.346
48	8	Absolute	60°	30°	0.360
49	4	Relative	30°	30°	0.208
50	6	Relative	30°	30°	0.246
51	8	Relative	30°	30°	0.272
52	4	Absolute	30°	30°	0.223
53	6	Absolute	30°	30°	0.243
54	8	Absolute	30°	30°	0.250

Table 2.8. (Cont.) The probabilities of detection for one tumor simulations are displayed.

2.4.7 Clinical Distribution of Tumors

The biopsy simulations were conducted a second time on more realistic geometric glands. By using a clinically derived distribution of number of tumors per gland, a better population was available for these biopsy simulations. A sample size of 1000 was again used but in this experiment, 1/4

of the glands had a single tumor, 1/2 had two tumors and the remaining 1/4 had 3 tumors. The total gland volume was again held to be less than 6.4 cc. This distribution is based on the analysis done by Daneshagari [2]. The ANOVA results are found in the Appendix and yield the same optimal biopsy procedure with a slightly different probability resulting from the factor effects model.

By using the values from this second table of effects, a probability for detection is calculated for the optimal setting:

$$\begin{aligned} \hat{Y}_{3131} &= \hat{\mu} + \hat{\alpha}_3 + \hat{\beta}_1 + \hat{\gamma}_3 + \hat{\delta}_1 + (\widehat{\alpha\beta})_{31} + (\widehat{\alpha\gamma})_{33} + (\widehat{\alpha\delta})_{31} + (\widehat{\beta\gamma})_{13} + (\widehat{\beta\delta})_{11} + (\widehat{\gamma\delta})_{31} \\ &= 1.7535 = 1.429 + 0.0733 + 0.01507 + 0.07456 + 0.07091 + \\ &0.02321 + 0.02650 + 0.01412 - 0.005442 - 0.004094 + 0.03638 \end{aligned}$$

Transforming this value (arcsine) yields a probability of detection for the optimal setting of .5908. This probability of 59.08% is higher than the 38.9% achieved by the simulation using geometric models of one tumor as would be expected. The predicted probabilities for each of the 54 experiments given this distribution of tumors is shown in Table 2.9.

Experiment	Treatment		Parameters		Predicted Probability
	Number of Needles	Spacing Method	θ	ϕ	
1	4	Relative	45°	45°	0.417
2	6	Relative	45°	45°	0.489
3	8	Relative	45°	45°	0.526
4	4	Absolute	45°	45°	0.417
5	6	Absolute	45°	45°	0.470
6	8	Absolute	45°	45°	0.482
7	4	Relative	60°	45°	0.427
8	6	Relative	60°	45°	0.524
9	8	Relative	60°	45°	0.569
10	4	Absolute	60°	45°	0.436
11	6	Absolute	60°	45°	0.514
12	8	Absolute	60°	45°	0.533
13	4	Relative	30°	45°	0.353
14	6	Relative	30°	45°	0.405
15	8	Relative	30°	45°	0.431
16	4	Absolute	30°	45°	0.354
17	6	Absolute	30°	45°	0.387
18	8	Absolute	30°	45°	0.388
19	4	Relative	45°	60°	0.358
20	6	Relative	45°	60°	0.408
21	8	Relative	45°	60°	0.443
22	4	Absolute	45°	60°	0.360
23	6	Absolute	45°	60°	0.391
24	8	Absolute	45°	60°	0.401
25	4	Relative	60°	60°	0.322
26	6	Relative	60°	60°	0.395
27	8	Relative	60°	60°	0.437
28	4	Absolute	60°	60°	0.332
29	6	Absolute	60°	60°	0.386
30	8	Absolute	60°	60°	0.403

Table 2.9. Given the distribution of one to three tumors, the probabilities of detection predicted by the ANOVA model are displayed.

Experiment	Treatment		Parameters		Predicted Probability
	Number of Needles	Spacing Method	θ	ϕ	
31	4	Relative	30°	60°	0.326
32	6	Relative	30°	60°	0.357
33	8	Relative	30°	60°	0.381
34	4	Absolute	30°	60°	0.329
35	6	Absolute	30°	60°	0.341
36	8	Absolute	30°	60°	0.340
37	4	Relative	45°	30°	0.417
38	6	Relative	45°	30°	0.498
39	8	Relative	45°	30°	0.541
40	4	Absolute	45°	30°	0.425
41	6	Absolute	45°	30°	0.486
42	8	Absolute	45°	30°	0.504
43	4	Relative	60°	30°	0.436
44	6	Relative	60°	30°	0.541
45	8	Relative	60°	30°	0.590
46	4	Absolute	60°	30°	0.451
47	6	Absolute	60°	30°	0.537
48	8	Absolute	60°	30°	0.562
49	4	Relative	30°	30°	0.351
50	6	Relative	30°	30°	0.412
51	8	Relative	30°	30°	0.444
52	4	Absolute	30°	30°	0.359
53	6	Absolute	30°	30°	0.401
54	8	Absolute	30°	30°	0.407

Table 2.9. (Cont.) Given the distribution of one to three tumors, the probabilities of detection predicted by the ANOVA model are displayed.

A selection of detection rates are graphed in Figure 2.7 to provide visualization of the relative ranking of various treatments. The plots indicate 6 and 8 needles, relative spacing and all of the levels for θ and ϕ .

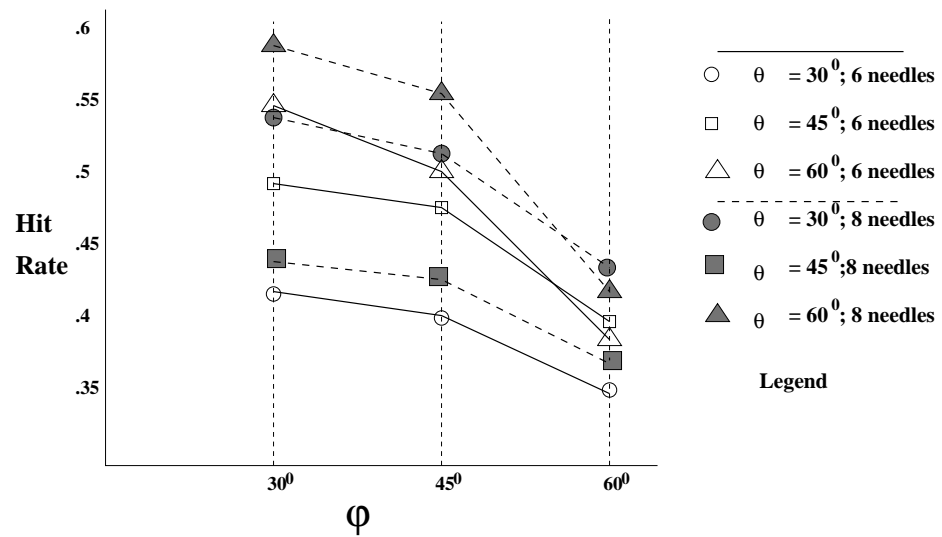


Figure 2.7. The detection rates for several experiments are graphed and the common treatment parameters are noted for each experiment. This gives a visual understanding of the ranking of these treatments in terms of their detection rate.

3. Digitized Specimen Data

3.1 Summary of Software Tool

An analysis program, written in C, was created to simulate needle biopsies on clinical data provided by the University of Colorado Health Sciences Center, Pathology Department. The clinical data were gathered from autopsies, pathologically investigated and digitized [2].

The data for each specimen are stored as a 3-dimensional array of information. The software uses an input file to determine the characteristics of a given experiment. These characteristics include the number of needles, the initial placement of the first needle, the angles θ and ϕ , the spacing between needles, and the needle diameter and length. In this manner, the analysis software is flexible enough to handle a variety of simulations. The goal of this biopsy simulation tool is to provide the means to experiment realistically with various needle parameters on clinical data in order to determine any correspondence between biopsy methods and detection rates.

The initial needle position is offset by the distance requested (the z -offset entered by the user), with half of the needles entering the right lobe

and the other half entering the left lobe, in symmetry with each other. The initial position is determined as an absolute (in cm) offset from the apex of the gland. The other parameters are used to position each needle on the specimen data set and determine how much of the specimen data is to be returned in the needle biopsy. This specimen data is analyzed to determine whether and how much tumor data is present in the needle. This information is available to the user.

Having read the input file with parameter values, the code begins a loop on the specimen data files requested for simulation. In this loop, the three-dimensional specimen data file is opened, the data are read into a 3-d array, with all of the background trimmed off, the apex of the gland is located, and the needle positions are translated into array coordinates. These coordinates are fed to the biopsy routine which extracts the specimen data coinciding with the needle and analyzes the data for tumor information. The information for the entire experiment is stored in an output file that documents the needle parameters and the results for each image data set.

3.2 Specific Algorithms

3.2.1 Locating the Apex

The apex is defined as the first contact with the prostate when approaching it through the rectum, as done clinically. This location is used as a landmark for positioning each biopsy needle. In the data set, the algorithm that searches for this landmark proceeds as follows. The planes are defined as shown in Figure 3.1.

Each pixel in the three-dimensional specimen file contains a number indicating the type of data at that location. The possible types are gland, tumor, capsule or background. Capsule data indicate those pixels defining the boundary of the gland. The apex is indicated by the first pixel pointing to capsule data. Therefore one plane of specimen data is evaluated at a time, until a pixel that points to capsule data is found. This location is recorded as the apex location.

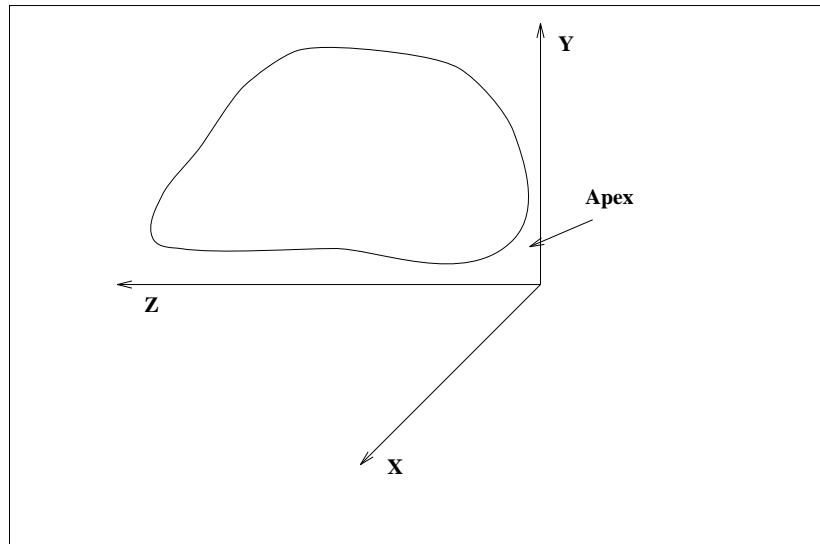


Figure 3.1. The x, y, z axis, as defined for the digital data, mimic those defined for the geometric models.

3.2.2 Establishing Needle Positions

The starting position, the location of the apex, serves as the landmark for each additional needle. From this starting point and the additional user-supplied parameters (z -offset, distance between needles) all of the needle positions are calculated in terms of a vector. This vector, represented by (x, y, z) coordinates, along with the ϕ angle, is a pointer to a specific pixel of image data. The z -offset is assumed to be in centimeters and is added to the initial (x, y, z) of the starting position to locate the first needle position. Each time any coordinate is changed, the new vector may be pointing to gland, tumor, background, urethra or capsule data. The pixel represented by the vector is read to insure that the needle entry position remains located on capsule data. If it does not, the y coordinate is adjusted to make sure that the entry position of the needle is on capsule data.

At this point in the algorithm, the first needle position is determined. There are two ways to space the remaining needles. The user may enter absolute distances in centimeters or a relative measure taken to be a percentage of the z dimension of the gland. In addition, a zero percentage indicates that

the spacing is based on the number of needles in the biopsy; the needles are equally spaced across the z -axis of the gland. The remaining needle positions are calculated from the initial needle position: half of the needles are positioned in the right lobe by using ϕ , the remainder use $-\phi$ to rotate into the left lobe. All of the needles have the x coordinate set to the midpoint of the gland in the x dimension.

The user-entered distance, in centimeters, is converted to a specific number of pixels. This z distance is added to the first needle position to obtain the second needle position, added to the second to obtain the third, etc. Each time a needle position is calculated, the coordinates are evaluated to insure that they point to capsule data. If the gland is too short in the z direction to handle all the needles requested, the experiment proceeds with the number of needles that do stay within the gland.

The experiments that depend on a relative distance between needles, require additional analysis of the yz slice before determining the z offset. The z diameter of the particular yz slice is calculated. The z distance required for a needle of a specific length, inserted at a specific angle is then subtracted from this z diameter. Rather than having the last needle pierce more background than gland data, this subtraction enables the full number of needles to be

inserted into the gland. This new z diameter is then divided into the number of segments required by the specified percentage. If the user indicates 0% for the distance spacing, the software calculates the distance based on the number of needles requested and the diameter of the yz plane.

3.3 Simulations

The 54 treatments used in the geometric model were used as biopsy procedures on a maximum of 53 digitized clinical specimens. Some of the biopsy techniques were simulated on only 52 of these clinical specimens. Table 3.1 shows the results from these simulations on the digitized clinical data. The table documents both the multiple-tumor geometric model hit rate as well as the number of hits resulting from the same biopsy on the digitized clinical data. The first five columns indicate the experiment number and the biopsy parameter settings for the four variables, number of needles, spacing method, θ and ϕ . The column labelled Detection Rate is the number of hits per 1000 simulations of the geometric model. The column labelled Number of Hits is the number of hits per number of digitized clinical samples. Most experiments were run on all 53 of the digitized specimens. However, some of the simulations resulted in an error on one or more of the specimens and these specimens were then removed from the experiment. The final column,

labelled Clinical Detection Rate is the rate for the experiments on the digitized specimens.

Experiment	Number of Needles	Spacing Method	θ	ϕ	Detection Rate	Number of Hits	Clinical Detection Rate
1	4	Relative	45°	45°	0.417	8	0.1509
2	6	Relative	45°	45°	0.489	53	0.2075
3	8	Relative	45°	45°	0.526	53	0.1538
4	4	Absolute	45°	45°	0.417	9	0.1698
5	6	Absolute	45°	45°	0.470	53	0.2075
6	8	Absolute	45°	45°	0.482	10	0.1923
7	4	Relative	60°	45°	0.427	9	0.1698
8	6	Relative	60°	45°	0.524	53	0.1731
9	8	Relative	60°	45°	0.569	53	0.2453
10	4	Absolute	60°	45°	0.436	10	0.1887
11	6	Absolute	60°	45°	0.514	53	0.2264
12	8	Absolute	60°	45°	0.533	53	0.2264
13	4	Relative	30°	45°	0.353	4	0.1321
14	6	Relative	30°	45°	0.405	53	0.2264
15	8	Relative	30°	45°	0.431	9	0.1698
16	4	Absolute	30°	45°	0.354	4	0.1321
17	6	Absolute	30°	45°	0.387	53	0.1321
18	8	Absolute	30°	45°	0.388	9	0.1698
19	4	Relative	45°	60°	0.358	6	0.1132
20	6	Relative	45°	60°	0.408	9	0.1698
21	8	Relative	45°	60°	0.443	53	0.2115
22	4	Absolute	45°	60°	0.360	8	0.1509
23	6	Absolute	45°	60°	0.391	10	0.1887
24	8	Absolute	45°	60°	0.401	53	0.1887
25	4	Relative	60°	60°	0.322	8	0.1509
26	6	Relative	60°	60°	0.395	8	0.1538
27	8	Relative	60°	60°	0.437	52	0.1731
28	4	Absolute	60°	60°	0.332	6	0.1154
29	6	Absolute	60°	60°	0.386	52	0.1731
30	8	Absolute	60°	60°	0.403	52	0.1731

Table 3.1 The detection rates for the geometric and clinical simulations are displayed.

Experiment	Number of Needles	Spacing Method	θ	ϕ	Detection Rate	Number of Hits	Clinical Detection Rate
31	4	Relative	30°	60°	0.326	$\frac{5}{52}$	0.0962
32	6	Relative	30°	60°	0.357	$\frac{5}{52}$	0.0962
33	8	Relative	30°	60°	0.381	$\frac{9}{52}$	0.1731
34	4	Absolute	30°	60°	0.329	$\frac{4}{52}$	0.0769
35	6	Absolute	30°	60°	0.341	$\frac{4}{52}$	0.0769
36	8	Absolute	30°	60°	0.340	$\frac{4}{52}$	0.0769
37	4	Relative	45°	30°	0.417	$\frac{6}{52}$	0.1154
38	6	Relative	45°	30°	0.498	$\frac{10}{52}$	0.1923
39	8	Relative	45°	30°	0.541	$\frac{12}{52}$	0.2308
40	4	Absolute	45°	30°	0.425	$\frac{8}{52}$	0.1538
41	6	Absolute	45°	30°	0.486	$\frac{10}{52}$	0.1923
42	8	Absolute	45°	30°	0.504	$\frac{11}{52}$	0.2115
43	4	Relative	60°	30°	0.436	$\frac{6}{52}$	0.1154
44	6	Relative	60°	30°	0.541	$\frac{10}{52}$	0.1923
45	8	Relative	60°	30°	0.590	$\frac{10}{52}$	0.1887
46	4	Absolute	60°	30°	0.451	$\frac{8}{53}$	0.1538
47	6	Absolute	60°	30°	0.537	$\frac{12}{52}$	0.2308
48	8	Absolute	60°	30°	0.562	$\frac{12}{52}$	0.2308
49	4	Relative	30°	30°	0.351	$\frac{3}{52}$	0.1000
50	6	Relative	30°	30°	0.412	$\frac{11}{52}$	0.2115
51	8	Relative	30°	30°	0.444	$\frac{10}{52}$	0.1923
52	4	Absolute	30°	30°	0.359	$\frac{6}{52}$	0.1154
53	6	Absolute	30°	30°	0.401	$\frac{8}{52}$	0.1538
54	8	Absolute	30°	30°	0.407	$\frac{10}{52}$	0.1923

Table 3.1 (Cont.) The detection rates for the geometric and clinical simulations are displayed.

3.4 Geometric Model vs Clinical Model

Comparison of the detection rates between the geometric model and the clinical model reveals that the geometric simulation produces much higher rates than its clinical counterpart. In attempting to explain this discrepancy, several characteristics of the experiment are noted.

The distribution of the tumors and the total tumor volume in a given specimen can impact the detection rate of a treatment. A comparison of the tumor volumes is graphically displayed in Figures 3.2 and 3.3. As shown by the histograms, the tumor volumes for the autopsy data tend strongly toward small ($\leq .5$ cc) volumes. In contrast, the geometric model produces tumors with volumes more equally spaced across the spectrum of possible volumes. In fact, 80% of the autopsy specimens have a total tumor volume less than .5 cc. In contrast, only 49% of the geometric gland models have a total tumor volume in this range. This difference in the size of the tumors can explain some of the difference in detection rate between the clinical and geometrical models.

A second difference is that the relative ranking of detection rates for the digital data simulations is different than the ranking of detection rates for the geometric simulations. An example of this discrepancy is that experiment 9, (8 Needles, Relative Spacing, $\theta = 60^\circ$, $\phi = 45^\circ$) achieved a detection rate of 0.2453 or 13 hits out of 53 samples. This detection rate is better than the detection rate of experiment 45, (8 Needles, Relative Spacing, $\theta = 60^\circ$, $\phi = 30^\circ$) which is the optimal biopsy as indicated by the geometric simulation. This difference may be due to the fact that only 53 specimens were used in the

digital simulation in contrast to the 1000 models constructed for the geometric simulation.

3.5 Optimal Technique vs SRSCB

The optimal technique, determined by the geometric model, consists of 8 needles, *relative* spacing, $\theta = 60^\circ$ and $\phi = 30^\circ$. The SRSCB procedure uses 6 needles, *absolute* spacing, $\theta = 45^\circ$ and $\phi = 45^\circ$. Both techniques were simulated on the geometric model as well as the digitized clinical data. The optimal technique actually proved slightly worse at tumor detection than the SRSCB procedure when simulated on the clinical data. In fact, the optimal method detected tumor in 10 out of 53 specimens (.189). The SRSCB method detected tumor in 11 out of 53 specimens (.207). These results compare with the overall results from the geometric simulation as follows. The SRSCB had a detection rate of .47 and the optimal had a detection rate of .59 on the 1000 geometric models. This discrepancy is addressed by noting the sample size available in the two simulations and the distribution of tumor volumes as noted earlier.

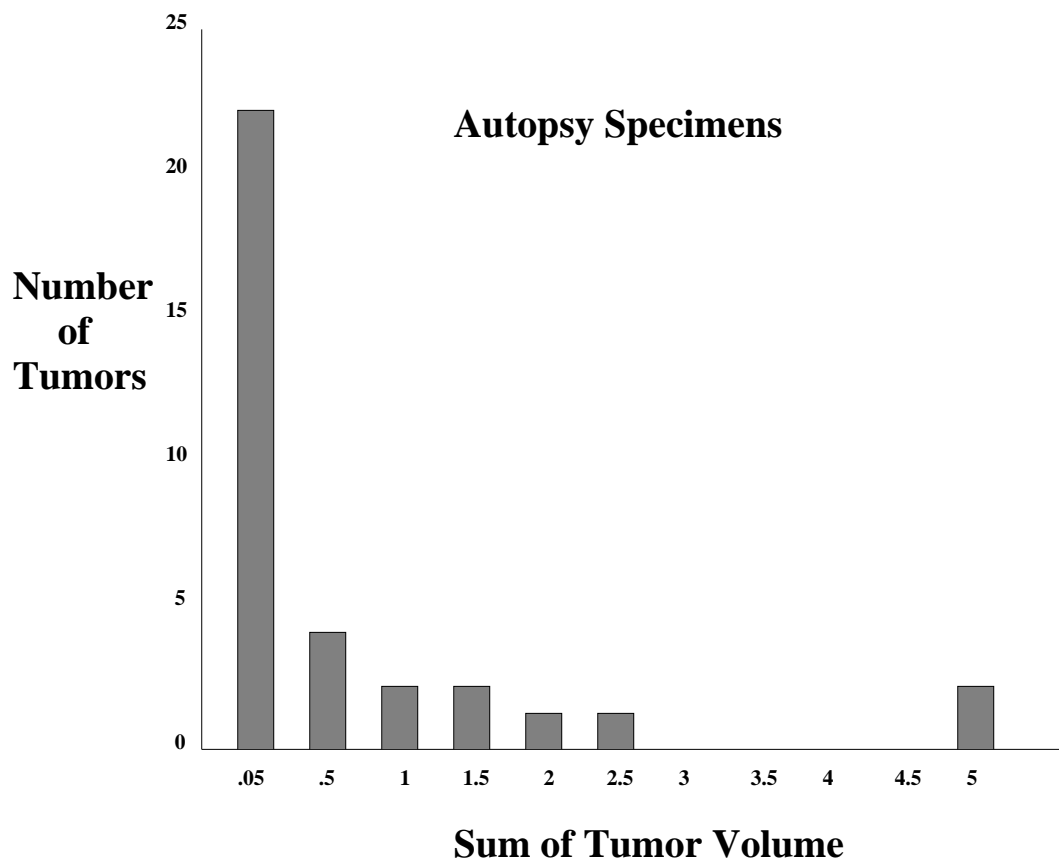


Figure 3.2. The histogram of the clinical data shows the tumor distribution by volume.

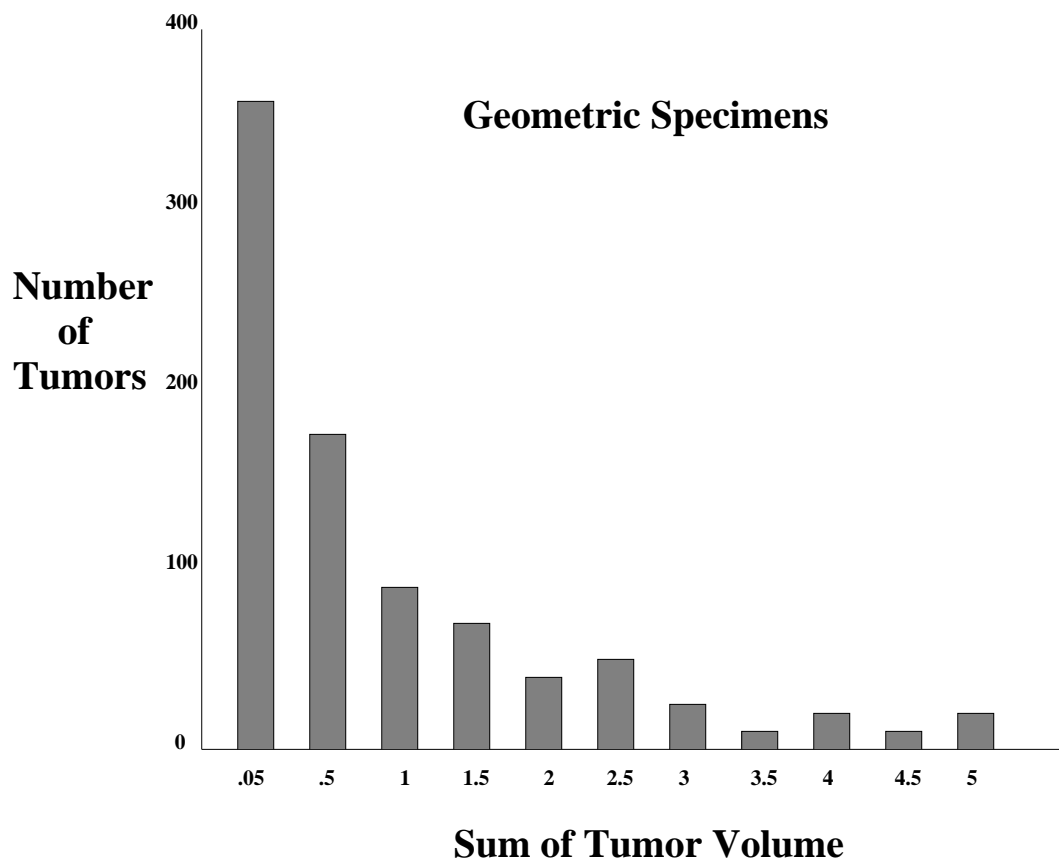


Figure 3.3. The histogram of the geometric data shows the tumor distribution by volume.

4. Geometric Model - Volume Estimates

4.1 Tumor Volume Estimates

The total volume of tumor in a gland is an important piece of information for clinicians who use it to improve both the diagnosis and treatment plan for a patient. The ultrasound used during a biopsy accurately measures the prostate gland volume so that an approximate ratio of tumor to gland volume can be used to estimate the volume of tumor in a gland. These simulations offered an avenue to explore a means of approximating this volume ratio by using the volume of the needle that contains tumor information and the total volume of the needle.

Three methods are used to estimate the amount of tumor intersected by the needle. The needle can be modeled by a line, a strip, or a cylinder in one, two, and three dimensions, respectively. The length and diameter of the needle are constant and are set by clinical limits. This incremental approach began in one dimension in order to simplify aspects of the simulation during software verification. As the research progressed, the two- and three-dimensional needles were introduced in order to model the actual biopsy more

closely.

The first method of estimating the volume ratio is $R = \frac{1}{n} \sum (\frac{v_i}{V_i})$ where v_i represents the tumor volume within a single needle, V_i represents the volume of that same needle, and n is the number of needles. This ratio is referred to as the average of the ratios. A second estimator of volume ratio is $r = \frac{\sum v_i}{\sum V_i}$, where v_i is the tumor volume within a single needle and V_i is the total volume of that needle. This ratio is considered the ratio of the average volumes since $\frac{1}{n} \sum_{i=1}^n v_i$ is the average tumor volume and $\frac{1}{n} \sum_{i=1}^n V_i$ is the average needle volume. This yields $r = \frac{\frac{1}{n} \sum v_i}{\frac{1}{n} \sum V_i} = \frac{\sum v_i}{\sum V_i}$. Both methods of estimating the ratio are documented below.

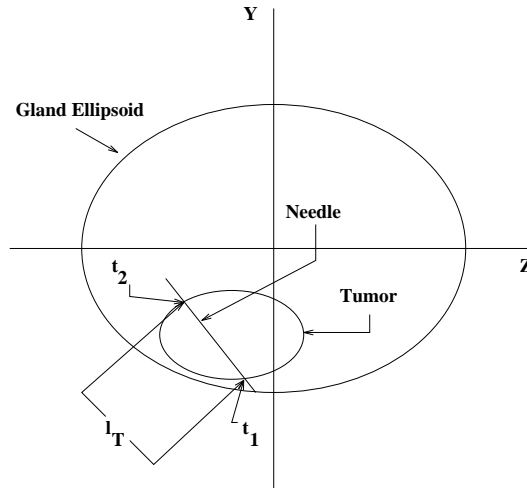


Figure 4.1. This illustration of the gland, tumor and one-dimensional needle depicts the variables used in determining the volume ratio estimator.

4.1.1 One-Dimensional Analysis - Line Model

In this first model, we represent the needle by a line segment as shown in Figure 4.1. The length of the needle that contains tumor pixels, l_T , is the difference between t_1 and t_2 , the two roots of equation (2.1): $l_T = | t_1 - t_2 |$. A needle length, L , of 1.25 cm is used in the estimate of volume ratio. Thus the ratio $\frac{l_T}{L}$ is an approximation of the true volume ratio $\frac{TV}{PGV}$; that is, $\frac{l_T}{L} \sim \frac{TV}{PGV}$.

4.1.2 Two-Dimensional - Strip Model

In the two-dimensional case we represent the needle by a strip. The needle entry points (x_0, y_0, z_0) are used as a starting point in the two-dimensional analysis. Two lines are created, each offset from this starting coordinate by the needle radius. The intersection between these two lines and the tumor ellipse is determined and the roots of the two resulting quadratics are used to compute both the occurrence of a detection and the amount of tumor within the needle. In this case, the estimate of the volume ratio is the area of the tumor over the area of the needle. Figure 4.2 defines the lengths used in determining the area. The area of the tumor is calculated by estimating the needle length which contains tumor data with the roots of intersection: $l_{t1} = | t_{11} - t_{12} |$; $l_{t2} = | t_{21} - t_{22} |$.

The area of tumor is then given by $a_T = \frac{d}{2}(l_{t1} + l_{t2})$ where d is the diameter of the needle. The area of the needle is calculated in the same way using the length of the needle: $a_N = \frac{d}{2}(L + L)$. Thus $\frac{a_T}{a_N}$ serves as an estimate of the true tumor to gland volume ratio, $\frac{TV}{PGV}$.

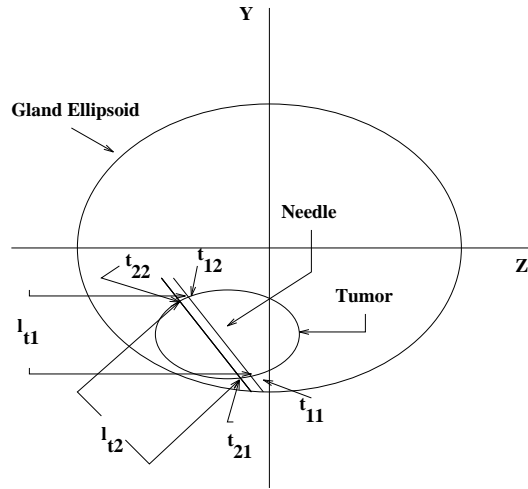


Figure 4.2. This illustration of the gland, tumor and two-dimensional needle depicts the variables used in determining the volume ratio estimator.

4.1.3 Three-Dimensional - Cylinder Model

The three-dimensional analysis models the needle as a cylinder and is similar to the two-dimensional case in that the entry point of the needle is again used as a center coordinate for four needles. In this case, the four needles are constructed symmetrically about this point to generate a cylindrical needle. Then intersections and roots are computed. A more accurate representation of the volume ratio is obtained using the volume of the tumor within the needle

over the volume of the needle. In this case, the length is estimated to be the maximum of the lengths determined from the four sets of intersection roots:

$$l_t = \max(|t_{11} - t_{12}|, |t_{21} - t_{22}|, |t_{31} - t_{32}|, |t_{41} - t_{42}|).$$

The volume of the needle depends on the known diameter and length: $v_N = \pi(\frac{d}{2})^2(L)$. The estimated volume of the tumor depends on the needle lengths which contain tumor data as shown in Figure 4.3. This leads to the tumor volume estimate $v_T = \pi(\frac{d}{2})^2(l_t)$. The ratio $\frac{v_T}{v_N}$ estimates the true volume ratio, $\frac{TV}{PGV}$.

4.2 Experiment Setup

A second set of experiments utilizing the geometric model involved exploring the question of accurately estimating the tumor volume to gland volume ratio. The experiment simulated a biopsy on a single specimen, increasing the number of needles each iteration and comparing the volume ratio obtained from the biopsy sample to the known volume ratio. The parameters for the biopsy include the optimal angles θ and ϕ determined from the ANOVA investigation. The optimal number of needles and distancing method determined from the ANOVA analysis do not apply to this experiment since the number of needles increases from 6 to 20 and the distancing of these needles is done so that the maximum number, 20, are equally spaced. The maximum number

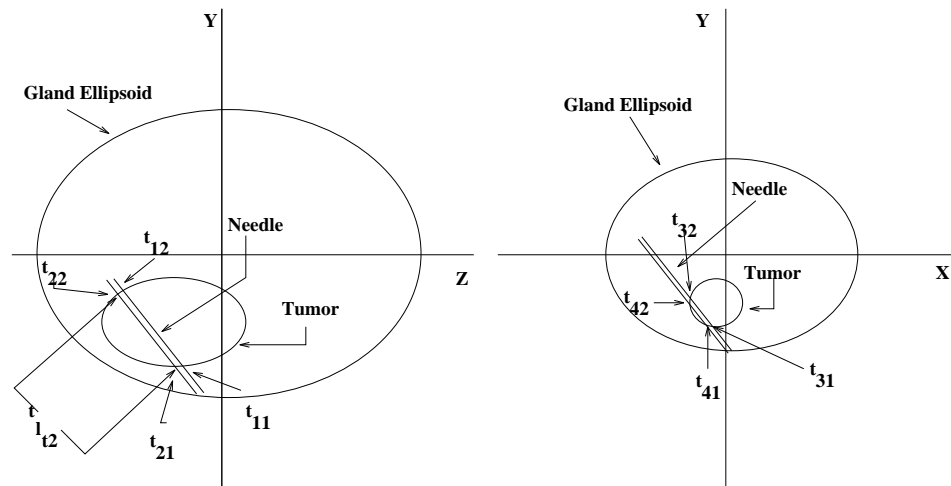


Figure 4.3. This illustration of the gland, tumor and three-dimensional needle depicts the variables used in determining the volume ratio estimator.

of needles was set at 20 due to clinical limitations. The spacing of the needles is dependent on the maximum number so that from one iteration to the next $n - 2$ needles are in the same exact location, yielding the same detection information. In this manner the comparison between a specimen biopsied by 6 needles and the same specimen biopsied by 10 needles is not dependent on needle position, but instead compares the gain made by the four additional needles.

The simulation is executed on 1000 specimens, varying the number of needles from 6 to 20 in increments of 2. The output from this experiment consists of a file for each specimen that contains the results of each set of needles including the tumor to needle volume ratio achieved and the associated estimates ($R = \frac{1}{n} \sum (v_t/v_n)$ and $r = \frac{\sum v_t}{\sum v_n}$). In addition, the actual tumor to gland volume ratio is noted.

4.3 Results

The results of this experiment were not as anticipated as there appears to be no pattern of convergence to the actual tumor to gland volume ratio within the limit of 20 total needles. However, much was learned from this exercise that provided insight into the next series of investigations. First, it is noted that in the great majority of cases, a single 8-needle biopsy tends

to overestimate the true tumor to gland volume ratio. Secondly, a comparison between the two methods of calculating the error leads to the conclusion that the sum of the ratios is the more accurate method at least in this set of limited trials.

4.4 Interactive Utility

Using the preceding idea as a starting point, an interactive software tool was created to investigate the volume ratio question in greater detail. This tool prompts the user for a random number, seeds the random number generator, creates a gland containing a single tumor and conducts the optimal 8-needle biopsy. This optimal biopsy has 8 needles, relative spacing between the needles, $\theta = 60^\circ$ and $\phi = 30^\circ$. The results, which include each needle position, the amount of tumor volume contained in the needle and an estimate as to the volume ratio of tumor to gland, are displayed for the user. At this point, the user is able to choose the location for the next needle. This new needle is then simulated and the tumor volume information it retrieves is incorporated into the volume ratio. The user can continue this process of requesting additional needles and evaluate the estimated volume ratio and its error from the true ratio. A maximum of 20 needles can be simulated on a single gland, beginning with the 8 original needles and accumulating the

additional 12 based on user specifications.

This area of research is full of open-ended questions where tools such as this interactive utility can help shed light on answers. With involvement from clinicians and medical researchers, experiments can be designed to gather more information regarding the two issues of volume ratio and optimal biopsy technique. In addition, using the results of this body of research, more realistic tumor distributions and geometric models can be constructed to better understand the impact of treatment parameters on detection rate.

A. APPENDIX ANOVA Definitions

A dot in the subscript indicates averaging over the variable represented by that index.

- The number of levels for *Number of Needles*: $a = 3$.
- The number of levels for *Distancing Method*: $b = 2$.
- The number of levels for θ : $c = 3$.
- The number of levels for ϕ : $d = 3$.
- The number of specimens = 1000.
- The number of experiments: $abcd = 54$.

In general, Y is an observation, \bar{Y} is the mean of observations, μ is the true mean and $\hat{\mu}$ is the least squares estimate of the true mean.

Y_{ijkl} is the observed detection rate at the factor levels indicated by i, j, k and l .

$\bar{Y}_{....}$ is the mean of all specimens over all treatment levels i, j, k, l . It indicates the overall detection rate for the entire experiment.

$$\bar{Y}_{....} = \frac{1}{abcd} \sum_{i=1}^a \sum_{j=1}^b \sum_{k=1}^c \sum_{l=1}^d Y_{ijkl}$$

$SSTO$, or total sum of squares is a measure of the total variability of the observations without consideration of factor level.

$$SSTO = \sum_{i=1}^a \sum_{j=1}^b \sum_{k=1}^c \sum_{l=1}^d (Y_{ijkl} - \bar{Y} \dots)^2$$

df_{SSTO} is the total degrees of freedom. The $SSTO$ has $abcd - 1 = 54 - 1$ degrees of freedom. One degree of freedom is lost due to the lack of independence between the deviations.

$SSTR$ or treatment sum of squares measures the extent of differences between estimated factor level means and the mean over all treatments. The greater the difference between factor level means (treatment means), the greater the value of $SSTR$.

$$SSTR = \sum_{i=1}^a \sum_{j=1}^b \sum_{k=1}^c \sum_{l=1}^d (\hat{Y}_{ijkl} - \bar{Y} \dots)^2$$

df_{SSTR} is the degrees of freedom. There are $r - 1$ degrees of freedom for the $SSTR$, where r is the number of parameters in the model. In the full model, $r = abcd = 54$, the total combinations of factor levels. In the model used for this simulation, $r = (a-1) + (b-1) + (c-1) + (d-1) + (a-1)(b-1) + (a-1)(c-1) + (a-1)(d-1) + (b-1)(c-1) + (b-1)(d-1) + (c-1)(d-1) = 26$. One degree of freedom is lost due to the lack of independence between the deviations.

SSE or error sum of squares, measures variability which is not explained by the differences between sample means. It is a measure of the variation within treatments. A smaller value of SSE indicates less variation within simulations at the same factor level.

$$SSE = \sum_{i=1}^a \sum_{j=1}^b \sum_{k=1}^c \sum_{l=1}^d (Y_{ijkl} - \hat{Y}_{ijkl})^2$$

df_{SSE} is the degrees of freedom. Since SSE is the sum of the errors across factor level, the degrees of freedom is the sum of the degrees of freedom for each factor level. It is the total number of simulations minus r , $abcd - r$.

MSE is the mean square for error defined by $MSE = SSE/df_{SSE}$. Note: The above definitions imply $SSTO = SSTR + SSE$. Due to this relationship, this process is referred to as the partitioning of the total sum of the squares.

In order to measure the variability within a factor level, the factor sum of square terms are computed. These terms are integral in the test statistic applied to determine whether a factor main effect is significant. In addition, interaction sum of squares are computed to measure variability of the interactions.

The factor A sum of squares corresponds to the *number of needles* factor.

$$SSA = bcd \sum_{i=1}^a (\bar{Y}_{i\dots} - \bar{Y}_{\dots})^2$$

Similar factor sum of squares are computed for each of the factors:

Factor	Sum of Square	Mean Sum of Square
Number of Needles	$SSA = bcd \sum_{i=1}^a (\bar{Y}_{i\dots} - \bar{Y}_{\dots})^2$	$MSA = SSA/(a - 1)$
Spacing Method	$SSB = acd \sum_{j=1}^b (\bar{Y}_{.j\dots} - \bar{Y}_{\dots})^2$	$MSB = SSB/(b - 1)$
θ	$SSC = abd \sum_{k=1}^c (\bar{Y}_{\dots k} - \bar{Y}_{\dots})^2$	$MSC = SSC/(c - 1)$
ϕ	$SSD = abc \sum_{l=1}^d (\bar{Y}_{\dots l} - \bar{Y}_{\dots})^2$	$MSD = SSD/(d - 1)$

The interaction sum of squares are computed as well for use in the F-test on the interactions. The first three pair-wise interaction sum of squares are shown below. The others are computed in the same manner.

Number of Needles: Spacing

$$SSAB = cd \sum_{i=1}^a \sum_{j=1}^b (\bar{Y}_{ij..} - \bar{Y}_{i...} - \bar{Y}_{.j..} + \bar{Y}_{....})^2$$

$$MSAB = SSAB / (a - 1)(b - 1)$$

Number of Needles: θ

$$SSAC = bd \sum_{i=1}^a \sum_{k=1}^c (\bar{Y}_{i..k.} - \bar{Y}_{i...} - \bar{Y}_{..k.} + \bar{Y}_{....})^2$$

$$MSAC = SSAC / (a - 1)(c - 1)$$

Number of Needles: ϕ

$$SSAD = bc \sum_{i=1}^a \sum_{l=1}^d (\bar{Y}_{i..l.} - \bar{Y}_{i...} - \bar{Y}_{..l.} + \bar{Y}_{....})^2$$

$$MSAD = SSAD / (a - 1)(d - 1)$$

The treatment means, μ_{ijkl} , indicate the mean for the treatment at the $ijkl$ levels of the respective factors.

The overall mean, μ , is the mean across all factors and all levels (across all i, j, k, l).

References

- (1) Hodge K.K., McNeal J.E., Terris M.K., Stamey T.A. "Random systematic versus directed ultrasound guided transrectal core biopsies of the prostate." *Journal of Urology* **142** (1989): 71-74.
- (2) Daneshgari, Firouz M.D., Taylor, Gerald D. PhD, Miller, Gary J. M.D., PhD, Crawford, E. David M.D. "Computer Simulation of the Probability of Detecting Low Volume Carcinoma of the Prostate with Six Random Systematic Core Biopsies". *Urology* **45** (April 1989): 604-609.
- (3) McNeal, John M.D. "Normal Histology of the Prostate" *The American Journal of Surgical Pathology* (1988): 619-633.
- (4) Neter, John, Wasserman, William, **Applied Linear Statistical Models**, Richard D. Irwin, Inc 1974.